The Astrophysical Journal, 811:88 (6pp), 2015 October 1 doi:10.1088/0004-637X/811/2/88

NONLINEAR DAMPING OF ALFVÉN WAVES IN THE SOLAR CORONA BELOW 1.5 SOLAR RADII

J. S. Zhao[1,2], Y. Voitenko[3], Y. Guo[4], J. T. Su[2], and D. J. Wu[1]
[1] Key Laboratory of Planetary Sciences, Purple Mountain Observatory, Chinese Academy of Sciences, Nanjing 210008, China
[2] Key Laboratory of Solar Activity, National Astronomical Observatories, Chinese Academy of Sciences, Beijing 100012, China
[3] Solar-Terrestrial Centre of Excellence, Space Physics Division, Belgian Institute for Space Aeronomy, Ringlaan-3-Avenue Circulaire, B-1180 Brussels, Belgium
[4] School of Astronomy and Space Science and Key Laboratory of Modern Astronomy and Astrophysics in Ministry of Education, Nanjing University, Nanjing 210046, China
Received 2015 June 14; accepted 2015 August 18; published 2015 September 24

ABSTRACT

Nonthermal velocities measured in the solar corona imply a strong damping of upward-propagating low-frequency $\lesssim$0.01 Hz Alfvén waves at heliocentric distances from 1.02 to 1.4 solar radii. We propose a vector Alfvén wave decay as a feasible mechanism for the observed Alfvén wave damping. Contrary to the extensively studied scalar decay, the vector decay does not depend on the wave frequency and can be efficient for low-frequency coronal Alfvén waves. We show that the vector decay is much stronger than the scalar decay and can provide the observed damping of 0.01 Hz coronal Alfvén waves with perpendicular wavelengths of $\sim 10^4$ km or less. Fully three-dimensional (3D) numerical simulations are needed to capture this decay, whose growth rate is proportional to the vector product of interacting wave vectors.

Key words: magnetohydrodynamics (MHD) – solar wind – Sun: corona – waves

1. INTRODUCTION

There are plenty of observations indicating that low-frequency Alfvén waves permeate the solar atmosphere and solar wind (e.g., De Pontieu et al. 2007; Banerjee et al. 2009; McIntosh et al. 2011; Bemporad & Abbo 2012; Hahn et al. 2012; Hahn & Savin 2013; Thurgood et al. 2014). These waves carry enough energy to heat corona and to accelerate fast solar wind (e.g., McIntosh et al. 2011). While Alfvén waves propagate upwards in the solar corona, their energy is gradually transferred to the coronal plasma and the wave energy flux should decrease with distance.

Signatures of the decreasing nonthermal velocity, which indicate the wave damping, have been seen in coronal holes by the *Solar and Heliospheric Observatory* (Harrison et al. 2002; O'shea et al. 2003) and recently confirmed by *Hinode* (Bemporad & Abbo 2012; Hahn et al. 2012; Hahn & Savin 2013). The latter works carefully checked the effects of stray light on the spectroscopic observations that were thought to be the possible reason for the decreasing nonthermal velocity (Dolla & Solomon 2008). Observations by Hahn et al. (2012) and Bemporad & Abbo (2012) suggest that starting from $\sim$30 km s^{-1} at the heliocentric distance $r = 1.02\ R_S$, the wave amplitudes first increase to a maximum $\sim$40 km s^{-1} at $r \sim 1.14\ R_S$, and then decrease to $\sim$20 km s^{-1} at $r \sim 1.4\ R_S$ (R_S is the solar radius).

For high-frequency Alfvén waves with periods $T \sim 1$ s, the main dissipation mechanism can be the collisional and Landau damping (e.g., Voitenko & Goossens 2000a, 2006; Dwivedi & Srivastava 2006), as well as the nonlinear decay of the Alfvén waves into themselves (e.g., Voitenko & Goossens 2000b). These high-frequency Alfvén waves can be excited by chromospheric reconnections if the scale is small (e.g., Axford & McKenzie 1992; McKenzie et al. 1995). However, large-scale Alfvén waves that have typical periods of $\sim$100 s can also be generated by the chromospheric reconnection events (Isobe et al. 2008). These long periods are consistent with periods of low-frequency Alfvén waves deduced from observations, $T \gtrsim 100$ s (see e.g., McIntosh et al. 2011; Thurgood et al. 2014). Here we will focus on the damping mechanisms of Alfvén waves with low-frequency $f \sim 0.01$ Hz. Most of the wave energy in the solar corona seems to be carried by these waves (Cranmer & van Ballegooijen 2005).

It is still unknown what mechanism dissipates 0.01 Hz Alfvén waves in the corona below 1.4 R_S. The direct damping mechanisms of the low-frequency Alfvén waves are collisional and collisionless (Landau) dampings. The collisional damping rate γ_c and Landau damping rate γ_L are (Voitenko & Goossens 2000a)

$$\gamma_c = 0.25\nu_e \frac{k_\perp^2 \lambda_e^2}{1 + k_\perp^2 \lambda_e^2}, \tag{1}$$

and

$$\gamma_L = \sqrt{\frac{\pi}{8}}\,\omega \frac{\rho_i^2 k_\perp^2}{\sqrt{1 + \rho^2 k_\perp^2}} \frac{T_e}{T_i} \frac{V_A}{V_{Te}}, \tag{2}$$

respectively, where $\nu_e = 4\sqrt{2\pi}\,\Lambda e^4 n_e \Big/ \left(3\sqrt{m_e}\,T_e^{3/2}\right)$ is the electron–ion collision frequency, Λ is the Coulomb logarithm, $\rho = \rho_i\sqrt{(T_i + T_e)/T_i}$, V_{Te} is the electron thermal velocity, and $k_\perp$ is the perpendicular wavenumber. Since collisional and Landau dampings weaken at longer wavelengths, they cannot efficiently dissipate low-frequency Alfvén waves at these scales (e.g., McIntosh et al. 2011). The corresponding damping rates for 0.01 Hz Alfvén waves are small, less than 5×10^{-2} of the angular wave frequency (see Figure 1), which means that the dissipation timescale is $\tau_d \sim 20$ times wave period. However, with the damping distance $L_d \simeq 0.18 \pm 0.04 R_S$ of the Alfvén wave in the lower corona (Hahn & Savin 2013), the damping timescale is nearly $\tau_d \sim R_d/V_A \sim 100$ s, which is of the same order as the wave period, indicating that the collsional and Landau damping cannot dissipate observed low-frequency Alfvén waves efficiently (Bemporad & Abbo 2012; Hahn et al. 2012; Hahn & Savin 2013).

The nonlinear decay of an outward Alfvén wave into an inward Alfvén wave and an outward slow wave (AAS decay)

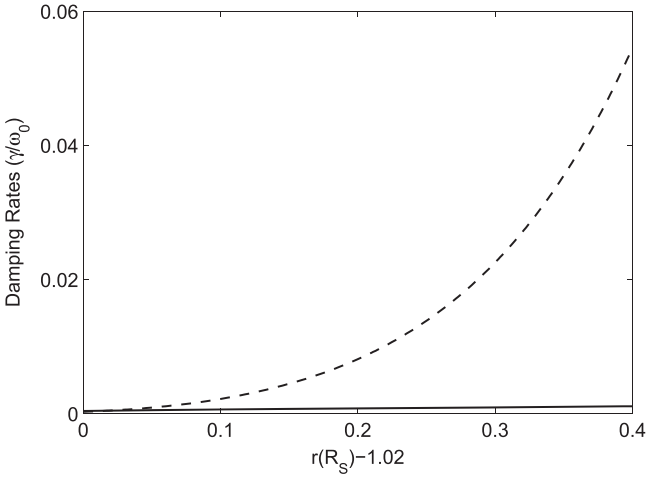

Figure 1. Radial distributions of collisional (γ_C, solid line) and Landau (γ_L, dashed line) damping rates of the low-frequency Alfvén wave with period $\tau = 100$ s, where Equation (4) is used to calculate the radial change of the perpendicular wavelength $\lambda_\perp(r)$ and $\lambda_\perp(r_1) = 1$ km is set at the boundary $r_1 = 1.02\ R_S$.

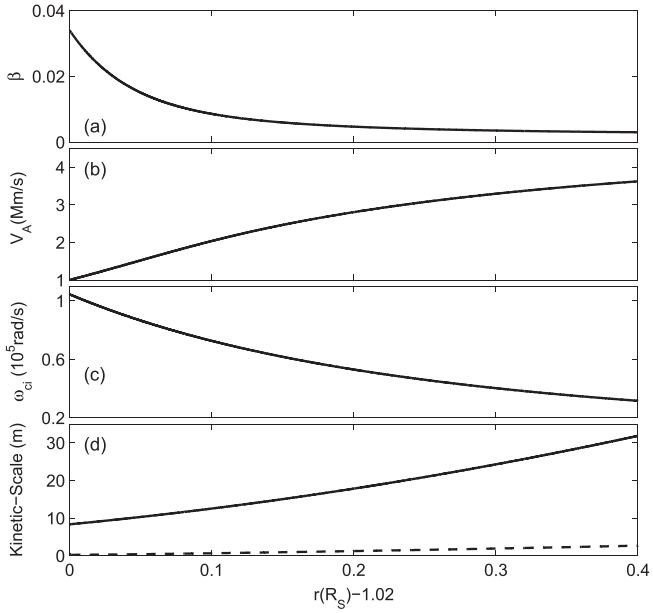

Figure 2. Plasma parameters in the solar corona from $r = 1.02$ to $r = 1.42$: (a) plasma β, (b) Alfvén speed V_A, (c) ion cyclotron frequency, and (d) ion gyroradius ρ_i (solid line) and electron inertial length λ_e (dashed line).

provides an interesting alternative to the linear damping mechanisms of Alfvén waves in the solar corona (e.g., Suzuki & Inutsuka 2005, 2006; Matsumoto & Suzuki 2012). Originally, the AAS decay was studied under the assumption that all three interacting waves propagate in the same plane (Galeev & Oraevskii 1963, and many authors cited later in this paper). However, this kind of decay (we call it the scalar decay) is too weak to explain the observed damping of low-frequency Alfvén waves at 1.02–1.4 solar radii. In the present study we propose an alternative vector-type AAS decay (Zhao et al. 2015) as a mechanism providing the observed decrease of the outward Alfvén wave flux at 1.02 and 1.4 solar radii.

2. PLASMA AND WAVE MODEL

We use the following electron number density model (Cranmer & van Ballegooijen 2005),

$$n_e(r) = 1.3 \times 10^{11} \times \left(\frac{1}{r^2} + \frac{25}{r^4} + \frac{300}{r^8} + \frac{1500}{r^{16}} + \frac{5796}{r^{33.9}}\right)\left(\mathrm{m}^{-3}\right), \quad (3)$$

the magnetic field strength model (Banaszkiewicz et al. 1998)

$$B_0(r) = 1.789 \times 10^{-4} \times \left(\frac{2}{r^2} + \frac{4.5}{r^5} + \frac{1}{1.538(r+1.538)^2}\right)(T), \quad (4)$$

and the electron temperature T_e model (Zhao et al. 2011)

$$T_e(r) = 4.2 \times 10^5\, re^{1-r/3} + 1.5 \times 10^5 (3/r)^{0.3}\ (\mathrm{K}). \quad (5)$$

We also assume equal electron and ion temperatures, $T_e = T_i$. Figure 2 presents the radial dependence of the plasma beta $\beta = k_B(T_e + T_i)/(m_i V_A^2)$, the Alfvén speed $V_A = B_0/\sqrt{\mu_0 n_e m_i}$, the ion cyclotron frequency $\omega_{ci} = eB_0/m_i$, the ion gyroradius $\rho_i = \sqrt{k_B T_i/m_i}/\omega_{ci}$, and the electron inertial length $\lambda_e = \sqrt{m_e/m_i}\,V_A/\omega_{ci}$.

In the solar corona the observed wave periods $T \gtrsim 100$ s (McIntosh et al. 2011) or 173 ± 118 s (Thurgood et al. 2014). With $T = 100$ s and $V_A = 2 \times 10^3\ \mathrm{km\ s^{-1}}$, the parallel wavelength $\lambda_\parallel$ can be estimated as $\lambda_\parallel = V_A T = 2 \times 10^5$ km. The perpendicular wavelength $\lambda_\perp$ and its radial evolution are difficult to infer from observations. We will use the fact that, because of the cross-$\boldsymbol{B}_0$ inhomogeneity of the Alfvén speed $V_A = V_A(x)$, the phase-mixing produces progressively smaller perpendicular wavelengths, in which case the radial dependence of $\lambda_\perp$ can be described as (Voitenko & Goossens 2006):

$$\frac{1}{\lambda_\perp(r)} = \frac{1}{2\,T}\int_{r_1}^{r} \frac{dx}{L_\perp(x)V_A(x)} + \frac{1}{\lambda_\perp(r_1)}, \quad (6)$$

where $L_\perp(r) = (B_0(r_1)/B_0(r))^{1/2} L_\perp(r_1)$ is the transverse width of the magnetic flux tube, and $B_0(r_1)$, $L_\perp(r_1)$, and $\lambda_\perp(r_1)$ are the magnetic field strength, the magnetic flux tube width, and the perpendicular wavelength, respectively, at the boundary $r = r_1$. In this study we consider the (most unfavorable) largest possible $\lambda_\perp$, fitting the tube width, $\lambda_\perp(r_1) = L_\perp(r_1)$, at the boundary $r_1 = 1.02$ (in units of solar radius).

3. NONLINEAR DECAY TYPES

Galeev & Oraevskii (1963) were among the first to show that a forward-propagating Alfvén wave can decay nonlinearly into a backward-propagating Alfvén wave and a forward-propagating slow magnetosonic wave (AAS decay). Through this decay, the energy of Alfvén waves propagating outward in the solar corona transfers to the outward slow waves and inward Alfvén waves. In turn, the Alfvén and slow product waves facilitate a dissipation of wave energy, Alfvén waves through the turbulent cascade to dissipation range (see the discussion in Section 4 and the references therein), and slow waves through kinetic wave-particle interaction and/or generating shocks (e.g., Suzuki & Inutsuka 2005, 2006; Matsumoto & Suzuki 2012). Therefore, the flux of outward Alfvén waves damps indirectly via the AAS decay.

We will distinguish between two decay types: scalar decay involving product waves propagating in the same plane as the pump wave, $\boldsymbol{k}_{j\perp} \times \boldsymbol{k}_{\perp} = 0$, and vector decay involving out-of-plain waves $\boldsymbol{k}_{j\perp} \times \boldsymbol{k}_{\perp} \neq 0$ (j stands for Alfvén or slow product wave). The formalism used by Galeev & Oraevskii (1963) allowed them to consider only the scalar AAS decay that was extensively studied later on (see, e.g., Zhao et al. 2014, and the references therein). To be efficient, the scalar AAS decay requires relatively large wave amplitudes, $\delta B/B_0 \gtrsim 0.3$. Such amplitudes can be reached in the outer corona and solar wind, but not in the corona below $1.5R_S$.

Recently, Zhao et al. (2015) investigated the two kinds of AAS decay, accounting for different nonlinearities, and found conditions when the vector-type ($\sim\left|\boldsymbol{k}_{j\perp} \times \boldsymbol{k}_{\perp}\right|$) nonlinearities dominate the scalar-type ($\sim\left|\boldsymbol{k}_{j\perp} \cdot \boldsymbol{k}_{\perp}\right|$) ones. Contrary to the scalar decay, the vector AAS decay can provide an efficient damping for low-frequency Alfvén waves with very small amplitudes $\delta B/B_0 \sim 10^{-3}$–$10^{-2}$.

The nonlinear decay rates corresponding to the scalar $\left(\gamma^s_{\rm NL}\right)$ and vector $\left(\gamma^v_{\rm NL}\right)$ effects are (Zhao et al. 2015)

$$\frac{\gamma^s_{\rm NL}}{\omega_{\rm ci}} \simeq \frac{1}{4(\beta/2)^{1/4}} \frac{\omega}{\omega_{\rm ci}} \times \frac{\left(K + K_1\right)^{1/2}}{\left(K_1 K_2 K^3\right)^{1/2}} \left|\hat{\boldsymbol{e}}_{t1} \cdot \hat{\boldsymbol{e}}_t\right| \left|\frac{\delta B}{B_0}\right| \quad (7)$$

and

$$\frac{\gamma^v_{\rm NL}}{\omega_{\rm ci}} \simeq \frac{1}{4(\beta/2)^{1/4}} \times \frac{\left(K + K_1\right)^{1/2}\left|K^2 K_1^2 - K_2^2\right|}{\left(K_1 K_2 K\right)^{3/2}} \left|\hat{\boldsymbol{e}}_{t1} \times \hat{\boldsymbol{e}}_t\right| \left|\frac{\delta B}{B_0}\right|, \quad (8)$$

where $K_j = \sqrt{1 + \rho^2 k_{j\perp}^2}$, $\hat{\boldsymbol{e}}_{tj} = \boldsymbol{k}_{j\perp}/k_{j\perp}$, and $j = 1$ and 2 for the inward Alfvén and outward slow waves (the pump outward Alfvén wave is given without a subscript). When the condition $\gamma_{\rm NL} \ll \omega_{1,2}$ is violated, the nonlinear decay rate is modified as (Galeev & Sagdeev 1979)

$$\gamma_{\rm mod} = \frac{\sqrt{3}}{2}\left(2\omega_2/\gamma_{\rm NL}\right)^{1/3}\gamma_{\rm NL}, \quad (9)$$

where $\gamma_{\rm NL}$ is $\gamma^s_{\rm NL}$ or $\gamma^v_{\rm NL}$.

In the weakly dispersive wavenumber range, $\rho^2 k_{j\perp}^2 < 1$, and taking into account the locality of the vector interaction in the wavenumber space, we estimate

$$\frac{\gamma^v_{\rm NL}}{\gamma^s_{\rm NL}} \sim \rho^2 k_\perp^2 \frac{\omega_{\rm ci}}{\omega}.$$

Therefore, the vector decay becomes stronger than the scalar decay at perpendicular wavenumbers

$$\rho^2 k_\perp^2 > \frac{\omega}{\omega_{\rm ci}}. \quad (10)$$

Figure 3 shows the vector (solid lines) and scalar (dashed lines) decay rates as functions of the perpendicular scale $\lambda_\perp^{(1)}$ at $r_1 = 1.02$ for two Alfvén wave amplitudes $\delta B^{(1)}/B_0 = \delta v^{(1)}/V_{\rm A} \sim 0.03$ (thick lines) and ~0.003 (thin lines). It is seen that the vector decay is efficient, $\gamma^v_{\rm NL}/\omega > 0.1$, for small amplitudes $\delta B^{(1)}/B_0 \sim 0.03$ at $\lambda_\perp^{(1)} \lesssim 10^4$ km, and for even smaller amplitudes $\delta B^{(1)}/B_0 \sim 0.003$ at $\lambda_\perp^{(1)} \lesssim 10^3$ km. Note that the scalar decay remains weak, $\gamma^s_{\rm NL}/\omega_0 \sim 10^{-2}$ in both cases. The extremely weak collisional (dash–dotted line) and Landau (dotted line) damping rates are shown for comparison.

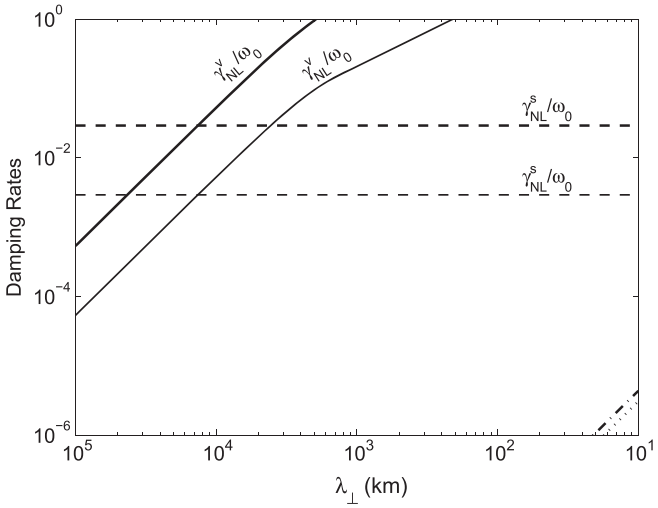

Figure 3. Vector (solid lines) and scalar (dashed lines) decay rates as functions of the wave perpendicular wavelength at $r = r_1 = 1.02$ R_S. Two wave amplitudes for low-frequency 0.01 Hz Alfvén waves are considered at $\delta v^{(1)} = 30$ km s^{-1} (thick solid and dashed lines) and $\delta v^{(1)} = 3$ km s^{-1} (thin solid and dashed lines). The collisional (dashed–dotted line) and Landau (dotted line) damping rates are given for comparison.

Next we consider the impact of the nonlinear decay on the radial dependence of the wave amplitude using a non-local estimation

$$\delta v(r) = C_1\left(n_{\rm e}(r)\right)^{-1/4} \exp\left(-\int_{r_1}^{r} \frac{\gamma(x)}{V_{\rm A}(x)}dx\right), \quad (11)$$

where $\gamma = \max\left[\gamma^s_{\rm NL}, \gamma^v_{\rm NL}\right]$, and $C_1 \equiv (n_{\rm e}^{(1)})^{1/4}\delta v^{(1)}$. We also consider four boundary values of the perpendicular wavelength of Alfvén waves, $\lambda_\perp^{(1)} = 10^5$, 1.5×10^4, 8×10^3, and 10^3 km. Since the phase-mixing (6) works as the Alfvén wave propagates outward from the Sun, the perpendicular wavelength will evolve to the smaller scale. The dependence of the perpendicular wavelength on the radial distance is shown in Figure 4 for different boundary conditions. The critical perpendicular scale λ_c is given by use of the relation, $\gamma^s_{\rm NL} = \gamma^v_{\rm NL}$. When the perpendicular wavelength is larger (smaller) than the critical scale, the scalar (vector) decay controls the Alfvén wave decay. Figure 4 shows the scalar decay dominating the Alfvén wave with $\lambda_\perp^{(1)} = 10^5$ km and the vector decay dominating the waves with $\lambda_\perp^{(1)} = 8 \times 10^3$ and 10^3 km. The Alfvén wave with $\lambda_\perp^{(1)} = 1.5 \times 10^4$ km goes from the scalar to vector decay at $r \sim 1.12$.

Figure 5 presents the Alfvén wave amplitude (11) as a function of r for four boundary values of the perpendicular wavelength, $\lambda_\perp^{(1)} = 10^5$, 1.5×10^4, 8×10^3, and 10^3 km. It is assumed that the initial amplitude $\delta v^{(1)} = 30$ km s^{-1} according to recent spectroscopic observations (e.g., Hahn et al. 2012; Hahn & Savin 2013). From Figure 5 one can see that the nonthermal velocities measured at radial distances $1.15 \lesssim r \lesssim 1.4$ by Hahn & Savin (2013) lie between the Alfvén wave amplitudes obtained from Equation (11) for $\lambda_\perp^{(1)} = 1.5 \times 10^4$ km and 8×10^3 km. Therefore, the observed

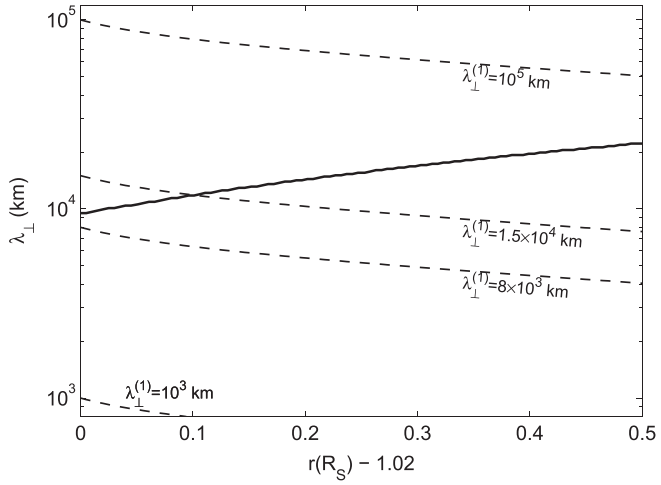

Figure 4. Radial dependence of the perpendicular wavelength of Alfvén waves resulting from the phase-mixing effect (6), where dashed lines denote four boundary values, $\lambda_\perp^{(1)} = 10^5$ km, 1.5×10^4 km, 8×10^3 km, and 10^3 km. The solid line represents the critical perpendicular wavelength λ_c for which $\gamma_{NL}^s = \gamma_{NL}^v$.

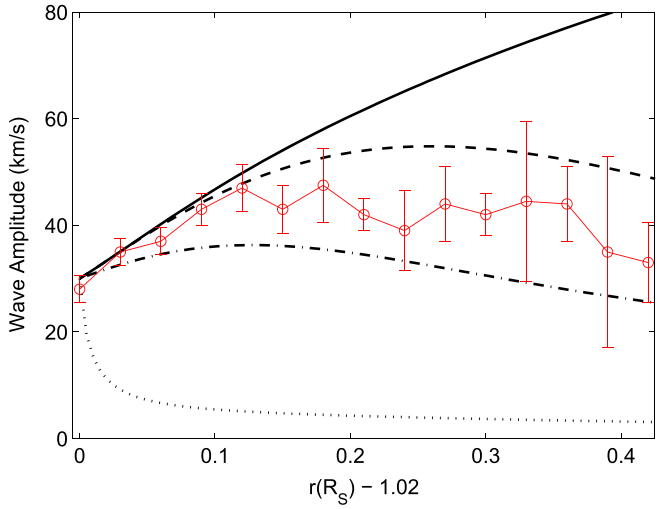

Figure 5. Radial dependence of the velocity amplitudes in low-frequency 0.01 Hz outward Alfvén waves with $\lambda_\perp^{(1)} = 10^5$ km (solid line), 1.5×10^4 km (dashed line), 8×10^3 km (dash–dotted line), and 10^3 km (dotted line) that resulted from the nonlinear decays. The solid line with error bars shows the nonthermal velocities measured by Hahn & Savin (2013).

decrease of the wave amplitudes with radial distance can be explained by the vector decay of Alfvén waves with $\lambda_\perp^{(1)} \sim 10^4$ km.

4. DISCUSSION

Here we did not consider the propagation of Alfvén waves from the source to the radial position $r\,(R_S) = 1.02$. The source of the coronal Alfvén waves can be sub-photospheric convection (e.g., Cranmer & van Ballegooijen 2005; Shelyag et al. 2013) and/or magnetic reconnection in the chromosphere (e.g., Isobe et al. 2008). These sources are labeled as "S1" and "S2" in Figure 6. When Alfvén waves excited by the convective motion propagate outward from the Sun, they encounter a sharp barrier at the transition region (e.g., Cranmer & van Ballegooijen 2005). Only ∼10% of the original wave flux $f_A = \delta v^2 V_A$ of the waves with $T = 3$ minutes can leak to

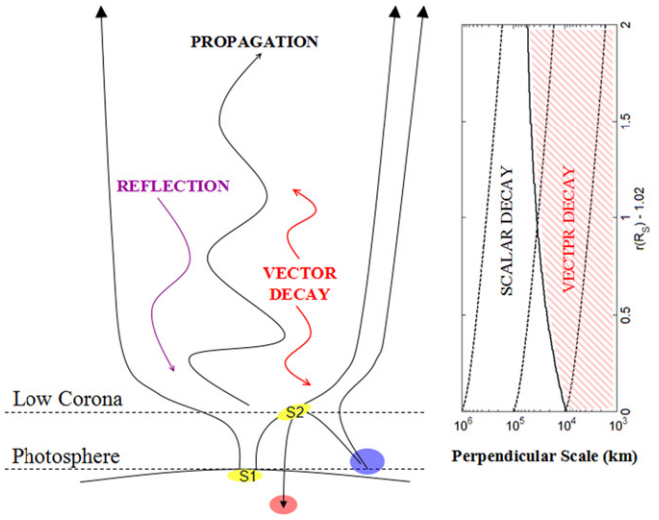

Figure 6. (Left panel): cartoon of Alfvén waves propagating in the coronal holes, where reflection and decay processes are shown. "S1" and "S2" denote the Alfvén wave sources for the convective motion below the photosphere and the reconnection in the chromosphere. (Right panel): the critical perpendicular wavelength λ_c for which $\gamma_{NL}^s = \gamma_{NL}^v$ (solid line) and perpendicular wavelengths $\lambda_\perp$ (dashed lines) that resulted from the phase-mixing as functions of the radial distance r starting from three boundary values $\lambda_\perp^{(1)} = 10^6$ km, 10^5 km, and 10^4 km at $r = r_1$. The vector-type decay dominates at $\lambda_\perp < \lambda_c$, while the scalar-type dominates at $\lambda_\perp > \lambda_c$.

the corona; for the shorter periods with $T = 3$ s, about 60% of the original flux can leak. However, the dominant component in the low corona is the waves with the periods of ∼1–3 minutes (Cranmer & van Ballegooijen 2005).

Also, we neglected the contribution of the products of inward Alfvén waves to the nonthermal velocity, assuming their fast damping by the turbulent cascade. Actually, the nonthermal velocity can be enhanced by the inward Alfvén waves at low altitudes close to the coronal base.

Inward Alfvén waves generated by vector AAS decay can interact with outward Aflvén waves and develop Alfvénic turbulence (e.g., Kraichnan 1965; Goldreich & Sridhar 1995; Matthaeus et al. 1999; Zhao et al. 2013). To estimate the efficiency of the cascade of the Alfvén wave turbulence, delivering the wave energy to the dissipation range, one has to estimate the cascade time from the injection scale to the dissipation scale where the waves damp fast. We assume a strong (critically balanced) turbulence (Goldreich & Sridhar 1995). At one cascade step the wave perpendicular scale decreases from $\lambda_\perp$ to $\lambda_\perp/2$ during the turnover time, which is nearly one wave period $2\pi/\omega(\lambda_\perp)$. The total cascade time is then $T_{cas} = \sum_{n=1}^{N} \frac{2\pi}{\omega(2^{n-1}\lambda_\perp)} \sim \sum_{n=1}^{N} \left(\frac{1}{2}\right)^{n-1} T_0 \sim 2T_0$, where T_0 is the wave period at injection and N is the number of cascade steps. A well-developed turbulence requires T_{cas} smaller than the Alfvén wave propagating from $r = 1.02$ to $r = 1.4$. With $T_0 = 100$ s, the wave energy can be dissipated effectively through the turbulent cascade mechanism.

Inward Alfvén waves can also be produced by the reflection of outward waves in the radially inhomogeneous solar corona. The inhomogeneity length scale $L_\parallel \equiv V_A\,(dV_A/dr)^{-1}$ is nearly larger than 10^5 km at the coronal base, and increases with the radial distance. Alfvén waves with $\lambda_\parallel \gtrsim L_\parallel$ are partly reflected. Note that the 0.01 Hz Alfvén wave with $\lambda_\parallel \sim L_\parallel$ at the coronal base undergoes a partial reflection. Far away from the coronal base where $\lambda_\parallel < L_\parallel$, the low-frequency Alfvén

wave propagates without reflection off of the radial inhomogeneity. At the same time, the density fluctuations of excited slow waves can result in the reflection of Alfvén waves (Suzuki & Inutsuka 2005, 2006). The collisions between the original outward and reflected inward Alfvén waves can develop the Alfvén wave turbulence (e.g., Matthaeus et al. 1999; Cranmer et al. 2007).

Outward Alfvén waves with wavelengths of $\lambda_{\parallel} < L_{\parallel}$ and $\lambda_{\perp} > L_c$ can propagate further into the outer corona and solar wind. The relative amplitude $\delta v/V_A \propto n_e^{1/4}/B_0$ increases with the radial distance in the outer corona and solar wind. When $\delta v/V_A$ reaches ~0.3, the scalar decay may become efficient at dissipating the waves. Magnetohydrodynamics (MHD) simulations suggest that the scalar AAS decay can occur in the solar corona at $r > 1.5$ (Suzuki & Inutsuka 2005, 2006; Antolin & Shibata 2010; Matsumoto & Suzuki 2012). The wave energy can be dissipated through two dissipation mechanisms, namely the shocks formed by slow waves and the Alfvén wave turbulence formed by the interaction between outward and inward Alfvén waves, which contribute to the coronal heating and solar wind acceleration (Suzuki & Inutsuka 2005, 2006; Antolin & Shibata 2010; Matsumoto & Suzuki 2012). However, whenever the Alfvén wave enters the vector decay regime (see dashed lines in Figure 6), the AAS vector decay will become much faster. The slow waves detected at the radial distances 1.5–20.5 R_s (Miyamoto et al. 2014) can therefore be generated not only by the scalar AAS decay (at higher frequencies) but also by the vector AAS decay (at oblique propagation).

Other nonlinear damping mechanisms for Alfvén waves may also occur. The nonlinear ponderomotive force induced by Alfvén waves can excite fast magnetosonic waves that dissipate through the shock formation (Nakariakov et al. 1997; Thurgood & McLaughlin 2013). Also, direct coupling between Alfvén and slow waves may occur at $\beta = 1$ (Zaqarashvili et al. 2006), which, however, is not typical for the corona where $\beta \ll 1$ (see Figure 2).

5. SUMMARY

The extensively studied AAS decay appears to be too slow to reduce the amplitudes of low-frequency ~0.01 Hz Alfvén waves between 1.02 and 1.5 solar radii to the level deduced from spectral line observations. This is because its growth rate is proportional to the wave frequency and becomes weak in the low-frequency range where the wave power is concentrated. However, most previous studies assumed that the Alfvén waves participating in the AAS decay propagate in the same plane, i.e., $|\boldsymbol{k}_{1\perp} \times \boldsymbol{k}_{\perp}| = 0$. In this case only terms $\sim \boldsymbol{k}_{1\perp} \cdot \boldsymbol{k}_{\perp}$ are taken into account, whereas terms $\sim|\boldsymbol{k}_{1\perp} \times \boldsymbol{k}_{\perp}|$ are neglected.

In fact, there are two kinds of nonlinear AAS decay: the scalar decay driven by nonlinearities $\sim \boldsymbol{k}_{1\perp} \cdot \boldsymbol{k}_{\perp}$ and the vector decay driven by terms $\sim|\boldsymbol{k}_{1\perp} \times \boldsymbol{k}_{\perp}|$ (Zhao et al. 2015). In the present paper we focused on the role of the vector decay. Contrary to the scalar decay, the growth rate of the vector decay depends not on the wave frequency (parallel wavelength), but on the perpendicular wavelength. Therefore, the vector AAS decay can be strong even at very low frequencies, provided the perpendicular wavelength of the Alfvén wave is sufficiently short. The condition that the vector decay dominates is nearly $\rho^2 k_{\perp}^2 > \omega/\omega_{ci}$.

We found that the vector AAS decay of Alfvén waves with frequencies ~0.01 Hz and perpendicular wavelengths $\lambda_{\perp} \lesssim 10^4$ km in the solar corona is stronger than the scalar one. Moreover, the vector decay in this wavelength range can become fast enough to explain the observed Alfvén wave damping.

With the boundary values of the Alfvén wave amplitude $\delta v^{(1)} = 30\ \mathrm{km\ s^{-1}}$ at $r = 1.02$, the expected amplitude of nondissipative Alfvén waves at $r = 1.4$ is $\delta v \gtrsim 100\ \mathrm{km\ s^{-1}}$, which is three times larger than the observed nonthermal velocities $\delta v_{nt} \approx 35\ \mathrm{km\ s^{-1}}$ (Hahn & Savin 2013). The scalar AAS decay, which was studied before, can only slightly reduce this value to about $80\ \mathrm{km\ s^{-1}}$, and other damping mechanisms are negligible. But the vector decay of Alfvén waves possessing perpendicular wavelengths $\lambda_{\perp}^{(1)} \sim 10^4$ km at the boundary limits the Alfvén wave amplitude to $\delta v \simeq 35\ \mathrm{km\ s^{-1}}$ at $r = 1.4$, which is compatible with the nonthermal velocities measured by Hahn & Savin (2013).

The vector-type nonlinearities not only accelerate the decay but also affect the spectral properties of generated waves, which may have observational consequences. One can mention here the spectral spread in azimuthal angle, which makes the wave polarization isotropic in the cross-$\boldsymbol{B}_0$ plane even if all of the initial waves are polarized in the same plane. However, the vector AAS decay could not be seen in the numerical simulations by Matsumoto & Suzuki (2012) because of the 2.5D model used. To account for essentially 3D vector decay one would need to use the fully 3D simulation model.

Finally, we should note that the broadband spectral distribution of Alfvén waves in the solar corona may reduce the nonlinear decay rate that is derived as the ideal condition for monochromatic waves and coherent interaction. More theoretical and simulation studies for the vector decay based on the broadband wave distribution are needed.

This research was supported by the Belgian Federal Science Policy Office via the Solar-Terrestrial Centre of Excellence IAP Programme (project P7/08 CHARM), by the European Commission via FP7 Program (project 313038 STORM), by NSFC under grant Nos. 11203014, 11303099, 11373070, 41074107, and 41531071, by MSTC under grant No. 2011CB811402, by the NSF of Jiangsu Province under grant No. BK2012495, by the Key Laboratory of Solar Activity at NAO, CAS, under grant No. KLSA201501, and by the Youth Innovation Promotion Association CAS.

REFERENCES

Antolin, P., & Shibata, K. 2010, ApJ, 712, 494
Axford, W. I., & McKenzie, J. F. 1992, in Solar Wind Seven Colloquium, ed. E. Marsch & R. Schwenn (Oxford: Pergamon), 1
Banaszkiewicz, M., Axford, W. I., & McKenzie, J. F. 1998, A&A, 337, 940
Banerjee, D., Pérez-Surez, D., & Doyle, J. G. 2009, A&A, 501, L15
Bemporad, A., & Abbo, L. 2012, ApJ, 751, 110
Cranmer, S. R., & van Ballegooijen, A. A. 2005, ApJS, 156, 265
Cranmer, S. R., van Ballegooijen, A. A., & Edgar, R. J. 2007, ApJS, 171, 520
De Pontieu, B., McIntosh, S., Carlsson, M., et al. 2007, Sci, 318, 1574
Dolla, L., & Solomon, Y. 2008, A&A, 483, 271
Dwivedi, B. N., & Srivastava, A. K. 2006, SoPh, 237, 143
Galeev, A. A., & Oraevskii, V. N. 1963, SPhD, 7, 988
Galeev, A. A., & Sagdeev, R. S. 1979, in Reviews of Plasma Physics, ed. M. A. Leontovich (Vol. 7; New York: Consultants Bureau), 1
Goldreich, P., & Sridhar, S. 1995, ApJ, 438, 763
Hahn, M., Landi, E., & Savin, D. W. 2012, ApJ, 753, 36
Hahn, M., & Savin, D. W. 2013, ApJ, 776, 78
Harrison, R. A., Hood, A. W., & Pike, C. D. 2002, A&A, 392, 319
Isobe, H., Proctor, M. R. E., & Weiss, N. O. 2008, ApJL, 679, L57
Kraichnan, R. H. 1965, PhFl, 8, 1385
Matsumoto, T., & Suzuki, T. K. 2012, ApJ, 749, 8

Matthaeus, W. H., Zank, G. P., Oughton, S., Mullan, D. J., & Dmitruk, P. 1999, ApJL, 523, L93
McIntosh, S. W., et al. 2011, Natur, 475, 477
McKenzie, J. F., Banaszkiewicz, M., & Axford, W. I. 1995, A&A, 303, L45
Miyamoto, M., Imamura, T., Tokumaru, M., et al. 2014, ApJ, 797, 51
Nakariakov, V. M., Roberts, B., & Murawski, K. 1997, SoPh, 175, 93
O'Shea, E., Banerjee, D., & Poedts, S. 2003, A&A, 400, 1065
Shelyag, S., Cally, P. S., Reid, A., & Mathioudakis, M. 2013, ApJL, 776, L4
Suzuki, T., & Inutsuka, S. 2005, ApJL, 632, L49
Suzuki, T., & Inutsuka, S. 2006, JGR, 111, A06101
Thurgood, J. O., & McLaughlin, J. A. 2013, SoPh, 288, 205
Thurgood, J. O., Morton, R. J., & McLaughlin, J. A. 2014, ApJL, 790, L2
Voitenko, Y., & Goossens, M. 2000a, A&A, 357, 1086
Voitenko, Y., & Goossens, M. 2000b, A&A, 357, 1073
Voitenko, Y., & Goossens, M. 2006, SSRv, 122, 255
Zaqarashvili, T. V., Oliver, R., & Ballester, J. L. 2006, A&A, 456, L13
Zhao, J. S., Voitenko, Y., De Keyser, J., & Wu, D. J. 2015, ApJ, 799, 222
Zhao, J. S., Voitenko, Y., Wu, D. J., & De Keyser, J. 2014, ApJ, 785, 139
Zhao, J. S., Wu, D. J., & Lu, J. Y. 2011, ApJ, 735, 114
Zhao, J. S., Wu, D. J., & Lu, J. Y. 2013, ApJ, 767, 109